JOURNAL OF AIRCRAFT
Vol. 29, No. 5, Sept.–Oct. 1992

Coining of Holes in Aluminum Plates: Finite Element Simulations and Experiments

Rutger Ogeman*
Chalmers University of Technology, Göteborg, Sweden

Stress coining is a cold working process used to create a compressive tangential stress field on the surface of a hole. Here, the development of stresses and strains in a 24-mm-thick aluminum plate during the coining of a hole is simulated in a nonlinear finite element analysis (FEA). The influence of different parameters on the residual tangential stresses, close to, and on the hole surface is studied numerically. These parameters are the coining depth, the mandrel diameter, the friction coefficient, the plate size, and the level of approximation in the FE-analysis. The three first parameters above are found to be the key parameters that control the residual stresses of interest. Experiments were performed to verify the results of the FE-computations by using resistance strain gauges on aluminum plates which contain a hole with a 27-mm diameter. Good agreement between measured and FE-calculated residual tangential and axial strains on the hole surface was obtained.

Nomenclature

E = Young's modulus of elasticity
n = exponent in Ramberg-Osgood constitutive law
T = plate thickness
ε_z = axial strain
ε_θ = tangential strain
ν = Poisson's coefficient
σ_{02} = stress at 0.2% strain offset
σ_c = contact stress
σ_{ult} = ultimate stress
σ_y = yield stress
σ_θ = tangential stress

Introduction

THE increased need for economic effectiveness in aviation and shipping operation demands higher payloads. One way to achieve the goal is to reduce the dead weight of the vehicle. A reduced weight and a high-fatigue resistance may be, but are not necessarily, conflicting issues, and fatigue failures, both severe and less serious, do occur.

Aeroplanes are subjected to high dynamic loads emanating mainly from starts and landings. In all real structures material and geometric discontinuities are present. In an aeroplane such discontinuities may appear at lightening holes, slots for cables or for fuel piping, etc. Stress concentrations arise in those areas and the risk for fatigue is thereby increased.

Small and fast ships are used in passenger transport, both on domestic and international routes. These types of ships are often built up of welded aluminum parts. During manufacturing, welding causes residual tensile and compressive stresses as a consequence of the local but high temperatures introduced. Both long range stresses of small magnitude, due to mounting misfit, and short range stresses of yield-stress magnitude, due to the heat deposition during welding, exist in the structure. The consequence of a combination of dynamic load and residual tensile-stresses is an escalated fatigue sensitivity.

Received Dec. 24, 1990; revision received July 6, 1991; accepted for publication Sept. 9, 1991.

*Research Assistant, Division of Marine Structural Engineering, S-412 96.

To achieve a higher weight effectiveness, the risk of fatigue failure must be reduced. There exist three main groups of methods to accomplish this[1]: 1) modification of the geometry so as to reduce the stress concentration; 2) the protection of the notch from the corrosive medium; and 3) modification of residual stress distribution caused by the manufacturing. This project deals with a residual stress method, coining, which belongs to the last group.

It is well known that residual stresses influence fatigue life. Favorable effects can be obtained, but also negative consequences arise. In the late sixties the aircraft industry started to develop residual stress methods capable of increasing the fatigue life several times over.[2] Coining methods[3–7] and mandrizing methods, where a conical or cambered mandrel is forced through the hole of interest,[6–9] were commonly used. All these methods intend to lower the resultant tensile stress by overstraining so as to produce a compressive stress state in the critical area. Due to the lowered tensile stresses, the fatigue life is enhanced. Recent work done in this field mostly concerns mandrizing methods, for example, split-sleeve hole expansion. Kasgard et al.[6] present experiments where residual tangential stresses at a hole in a thin aluminum plate are determined after coining. A summary of residual stress methods is presented by McNeill-Heston.[7]

Present Investigation

The present investigation has two aims: to demonstrate the use of finite element analysis as a tool to simulate the build-up of stresses and strains in a plate during a stress coining process, and to identify the main parameters controlling the residual stress state in the plate. The coining process studied here is shown schematically in Fig. 1. The plate that contains the hole to be coined is placed between two steel mandrels which are pressed together. The plate materials used in this investigation are two different tempers of an aluminum alloy, AA6082-T6, and annealed AA6082. However all results for the annealed AA6082 plates are presented by Ogeman[10] which is an extended version of the presented paper. In the FE-simulations, the influence of the plate size, the coining depth, the mandrel diameter, the friction coefficient between the mandrels and the plate, and the level of approximations in the FE-model on the residual stress state in the plate is quantified.

Several experiments are also performed to verify the capability of the FE-model to accurately compute strains during a coining process.

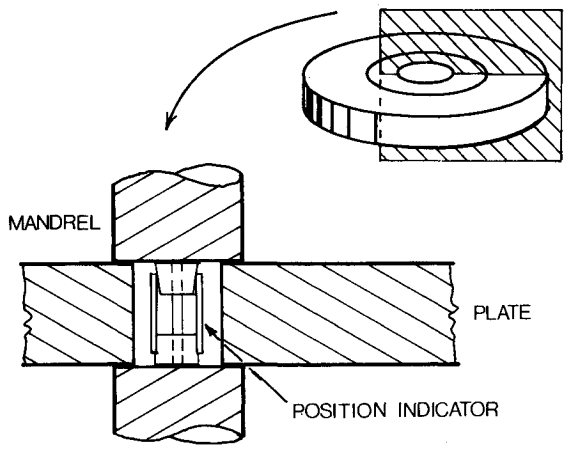

Fig. 1 Schematic representation of the coining process.

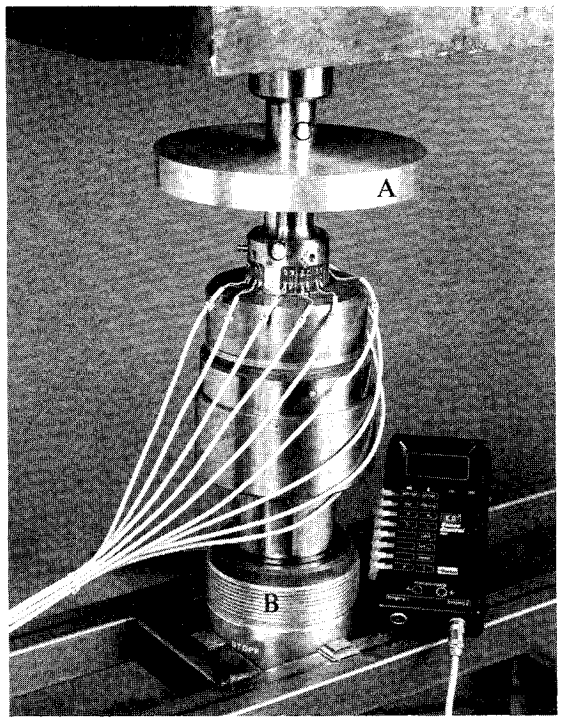

Fig. 2 Coining test equipment: a) test plate; b) hydraulic cylinder; and c) mandrels.

Coining Experiments

The cold working process used in this investigation is a type of coining process. Two polished 35-mm-diam high strength steel mandrels are pressed together with an aluminum test-plate placed in between, see Figs. 1 and 2. One of the mandrels is fixed in a rigid frame. The other mandrel is mounted on a spherical bearing connected to a 400 kN hydraulic cylinder which is controlled by a high-pressure pump.

The test material used in this investigation is 25-mm-thick plates made of AA6082-T6 aluminum. Typical tensile properties for AA6082-T6 are $\sigma_{02} = 290$ MPa and $\sigma_{ult} = 322$ MPa. The mandrels are manufactured from a high strength steel, with $\sigma_y = 850$ MPa, $\nu = 0.3$ and $E = 210$ GPa. All test plates are taken from the same sheet, and they are heat-treated separately in a furnace. The test plates have a diameter of 200 mm. The holes are first drilled to approximately 20-mm diameter and then turned to 26.50 mm. The plates are turned within a diameter of 80 mm on both sides to obtain a uniform thickness of 23.9 mm. Care is taken to control the temperature during manufacturing to avoid the development of temperature-induced residual stresses. The present paper presents results from test plates Nos. 3, 4, 5, 6, 13, 14, and 15. Test plates 1 and 2 were used to adjust the testing equipment and test plates 7, 8, 9, 10, 11, 12, 16, and 17 are made of different tempers.

To accurately measure the relative vertical displacement of the mandrels, a special position indicator is designed and placed inside the hole between the mandrels, see Fig. 1.

To ensure a concentric placing of the plate and the mandrels before the coining process starts, a fixture is used. After the first load step, the fixture is released, so as not to influence the behavior of the test plate during coining.

At each load step, the relative vertical displacement of the mandrels and the total strain at 8 different locations on the surface inside the hole (hole surface) are measured. The strains are measured with strain gauges each covering an area of 1.4 $\times$ 4.0 mm. They are placed to form three groups equally spaced (spacing, $\theta = 120$ deg), see Fig. 3. Gauges 10, 12, and 14 are situated 5.35 $\pm$ 0.1 mm below the plate upper surface, tangentially oriented (θ-dir). Gauges 11, 13, and 15 are placed tangentially in the center-plane of the plate. Gauge 16, located 5.35 $\pm$ 0.1 mm below the plate's upper surface and gauge 17, in the center plane, are vertically oriented (z dir). Gauge 17 is present only on test plates Nos. 13, 14, and 15. The force on the test plate is increased in steps of 6.3 kN until a noticeable nonlinear behavior is observed, and then the step size is decreased to 3.15 kN. The load is increased until the total compression of the plate is 0.350 mm, equivalent to 1.5% for the 25-mm-thick plate. This corresponds to $\sigma_c = 580$ MPa, which is twice the yield stress level for AA6082-T6. After loading to maximum compression, the load is released in two or three steps, and then the test plate is removed.

The residual displacements perpendicular to the contact surface and perpendicular to the hole surface, are measured with a dial test indicator.

Finite Element Analysis: Introduction

In this investigation, a commercially available FE-code for nonlinear calculations, SOLVIA,[11] is used. Different kinds of nonlinear effects such as material nonlinearities, geometrical nonlinearities, and contact conditions can then be accounted for.[12] Geometrical nonlinearities can be modeled as large displacements but small strains, as in the case of large motions of plate-like structures, or as large displacements and large strains as in metal forming.

Calculation Procedure

The model in this study has a simple geometry: a circular plate with a central hole partly covered by two circular mandrels, see Fig. 4. Due to the axial symmetry, the model can be treated as two-dimensional, which drastically reduces the size of the FE-model. Axisymmetric eight-node isoparametric elements are used in this study. The axisymmetric element provides the stiffness of a part of the structure that covers 1

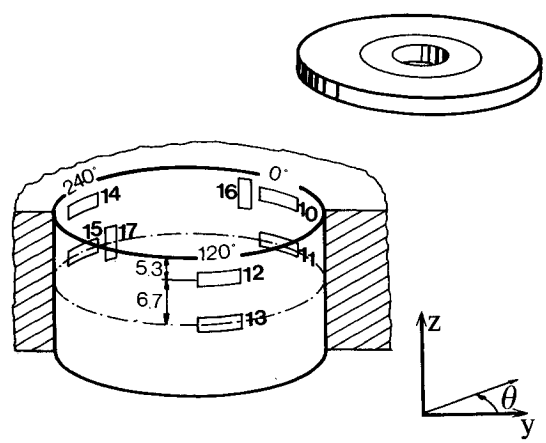

Fig. 3 Strain gauges located inside the hole.

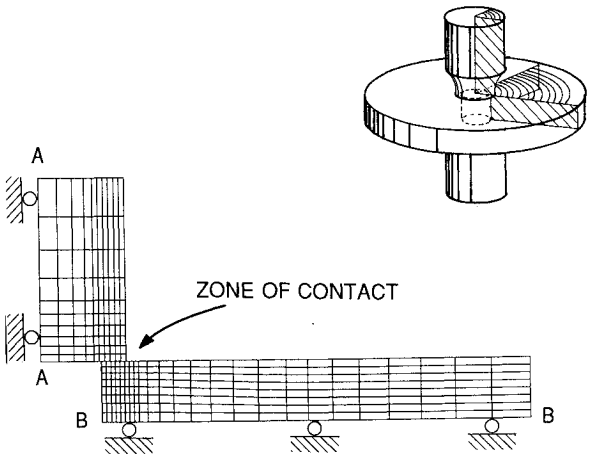

Fig. 4 Axially symmetric finite element model with boundary conditions used. Lines A–A and B–B are lines of symmetry.

radian in the tangential direction. The plate and the load also have a horizontal plane of symmetry, hence, using appropriate boundary conditions, only half the model needs to be studied. Figure 4 shows the axially symmetric FE-model together with the boundary conditions used. The integrals in the element stiffness matrices are calculated with 2×2 or 3×3 Gaussian points. In the zone where the mandrel and the plate touch the FE-code considers possible contact with nonzero friction between the two surfaces. The magnitude of the friction coefficient is taken from experiments described in Ogeman.[10] Full Newton-Raphson iterations are used in the equilibrium equations to establish force equilibrium at the end of each load step when contact surfaces are present. The resulting system of equations that governs the iterations for the fulfillment of force equilibrium and contact conditions at the end of a time step is derived in Bathe.[12]

The calculations showed that it was sufficient to use default values in the FE-code SOLVIA to reach equilibrium in the nonlinear analysis. Hence, convergence is assumed to be reached when the increment in internal energy is less than 0.001 times the initial incremental energy in the first iteration of that load step. When contact-surfaces are present, additional contact-force convergence criteria are also used. To reach convergence, the difference in the absolute value of the out-of-balance contact-force vector between two consecutive iterations must be less than 5% of the absolute value of out-of-balance contact-force vector from the previous iteration.

The load is applied as a load-history where the displacement of the upper surface of the mandrel is prescribed. The load-history consists of 30–40 load steps, of which 20 describe the loading phase and the rest the unloading phase. The maximum prescribed displacement of the mandrel is 0.350 mm, which is the same as in the experiments.

Material Model

The Ramberg-Osgood law is often used to describe the elasto-plastic stress-strain behavior for aluminum because the predicted behavior approximates the real behavior of most alloys[13]

$$\varepsilon = (\sigma/E) + 0.002\,(\sigma/\sigma_{02})^n$$

For heat-treated alloys n varies from 20 to 50. With $n = 50$ and $\sigma_{02} = 307$ MPa the Ramberg-Osgood law simulates the fully heat-treated AA6082-T6 uni-axial stress-strain behavior very closely.

The nonlinear material input for the FE-calculations is given as a uni-axial stress-strain curve which is divided into linear segments. For AA6082-T6, four points on the Ramberg-Osgood curve are used. Most aluminum alloys show an ideal kinematic Bauschinger effect during strain-hardening.[13] Thus, kinematic strain-hardening is assumed in the present FE-calculations. Furthermore, in the FE-calculations the von Mises yield criterion and an associated flow rule are employed.

Numerical Modeling

To verify the assumption that a materially nonlinear-only analysis is sufficient for the modeling of the coining process, a 139-element mesh is designed. The parameters varied in these calculations are: 1) small or large displacement theory, 2) small or large strain theory, 3) isotropic or kinematic hardening rules, 4) the number of integration points in the elements for calculation of stiffness matrices and load vectors, and 5) the shape of the stress-strain curve for the material. (For a certain total strain value the stress value is changed 5%.) In all, 36 combinations of the parameters described are investigated in the FE-calculations. Only marginal differences are found in the calculated stress and strain fields between the results from these different computations. For example, the calculated accumulated effective plastic strain in the plate differs less than 10%, and the tangential residual stress (although not the same stress measure) differs less than 15% using large displacements and large strains theory instead of materially nonlinear-only theory. The cpu-time needed increases when large strains and large displacements are accounted for. Accordingly, to obtain effectivenss in the following calculations, a materially nonlinear-only theory is used. A 292 element mesh and a 444 element mesh are also designed and used to verify the assumption that the effect of nonlinear behavior is approximately independent of the number of elements in the mesh. No sign of a stronger dependency on the nonlinear behavior is observed.

A study of the convergence of the FE-calculations reported in Ogeman,[10] shows that a 292-element mesh is sufficient for this investigation. Hence, in the following calculations the 292-element mesh is used. In this mesh, the mandrel which is assumed to be elastic, consists of 100 linear elastic elements. For the complete 292-element mesh the total number of equations equals 1900. The computations are performed on a Digital MicroVAX 3500 computer. The cpu-time needed for the execution of one load-history is about $2\frac{1}{2}$ h.

To estimate the accuracy of FE-calculated results, the deviation of the maximum von Mises effective stress between a value from a Gaussian point that is located closest to a nodal point and the nodal mean value can be used as long as the plastic strains remain small and the material remains essentially elastic. The deviation in the von Mises effective stress varies from less than 1% to 23% in different parts of the plate. In the plate, close to the corner of the mandrel, the stresses are singular, which disqualifies the use of the deviation of the stresses as an estimate of accuracy in these parts. However, close to the hole surface, an area of interest for this study, the stress deviation is less than 5%, and here the material shows almost purely elastic behavior.

Results

The results presented below are divided into three parts: part 1, where the measured strains and displacements are compared with the numerically calculated strains and displacements; part 2, where FE-computed stresses and strains at certain locations in the plate are presented; and part 3, where the influence on the residual tangential stresses of certain physical parameters, for example the coining depth, are calculated by use of FEA.

Measured and Computed Strains

The experimental strain results presented here are estimated mean values from measured strain values for gauges 10, 12, and 14, denoted $\varepsilon_{\theta 1}$ and for 11, 13, and 15, denoted $\varepsilon_{\theta 2}$. This will reduce the effect of material and geometrical discontinuities. From gauges 16 and 17 only single strain-values are presented. These strains are denoted ε_{z1} and ε_{z2} in the text below (see also Fig. 3). The size of the gauges implies that the corresponding strain values from the FE-

calculations have to be estimated mean values emanating from several Gaussian points. Hence, $\varepsilon_{\theta 1}$ and ε_{z2} are mean values estimated from two Gaussian point values; ε_{z1} is estimated from four Gaussian point values, and $\varepsilon_{\theta 2}$ is calculated from a single Gaussian point value. It should also be noted that the Gaussian points are situated inside the hole surface, for the 2 × 2 Gaussian points mesh the distance is about 0.20 mm. Figure 5 shows the measured $\varepsilon_{\theta 1}$ vs the coining-force for tests 5, 6, 13, 14 and for the FE-calculations. Similarly, Figs. 6–8 show $\varepsilon_{\theta 2}$, ε_{z1}, and ε_{z2}. Because of failures on reaction force measurements equipment during the experiments, test plate 15 has been eliminated. The strain results from test plates 3 and 4 are omitted in the diagrams because the tangential and axial strains show less scatter than tests 5, 6, 13, and 14.

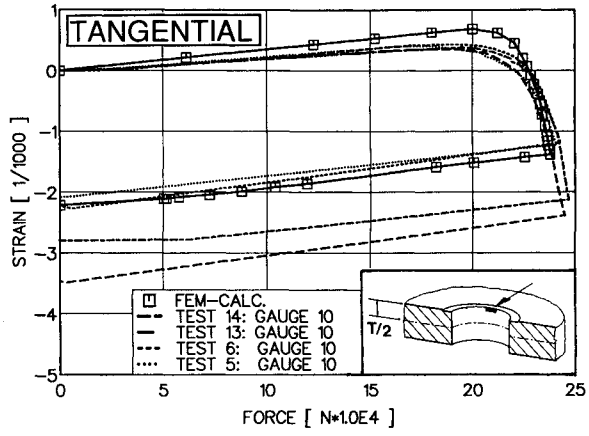

Fig. 5 Measured tangential strain $\varepsilon_{\theta 1}$ vs coining force for test plates 5, 6, 13, 14 together with corresponding calculated FE-results.

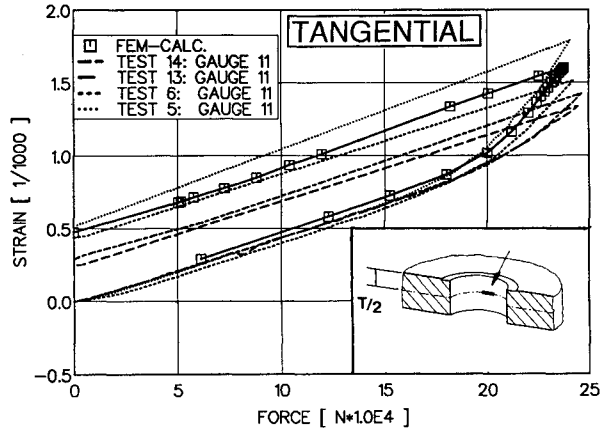

Fig. 6 Measured tangential strain $\varepsilon_{\theta 2}$ vs coining force for test plates 5, 6, 13, 14 together with calculated corresponding FE-result.

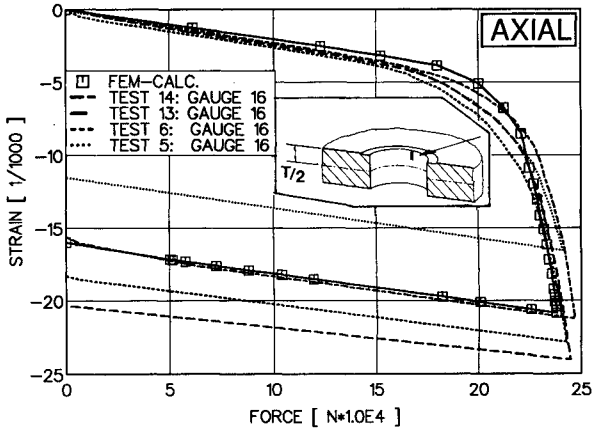

Fig. 7 Measured axial strain ε_{z1} vs coining force for test plates 5, 6, 13, 14 together with corresponding calculated FE-result.

The FE-computations result in a strain vs coining-force curve which is close to the curves from the experiments (see Figs. 5–8). The largest observed difference between the FE-calculated and the measured strains is about 45%. This discrepancy appears for $\varepsilon_{\theta 2}$ in test plate 13 after unloading. The scatter in measured strain for each test, between gauges located at θ = 0, θ = 120, and θ = 240 deg is less than the scatter in measured strain between the different tests shown in Figs. 5–8.

Measured and Computed Displacements

Figure 9 shows estimated mean values and ± one standard deviation (Sdev) for the measured hole profile of test plate 13, before and after coining has been performed. It also shows the FE-calculated profile after coining. To obtain sufficient accuracy all the hole profiles are measured twice. Measurements are performed on both sides and at three locations: θ = 60, θ = 180, and θ = 300 deg. The maximum difference between the calculated and the measured displacements, close to the plate surface, is about 20%. There is a good agreement between the FE-calculated and the measured displacements for the remaining part of the hole surface.

The measured residual stress state at a point is calculated from the residual elastic strains in the same point. The elastic strains are calculated as the difference between maximum values and unloaded values if no plastic strains occur during unloading. Hence, the accuracy of the measured elastic strains are important for this study. Accordingly, mean values and standard deviations are estimated for the elastic strains during unloading at two locations, gauges 10, 12, 14 and gauges 11, 13, 15, for tests 5, 6, 13, and 14. Also for strains at maximum load, mean values and standard deviations are estimated at

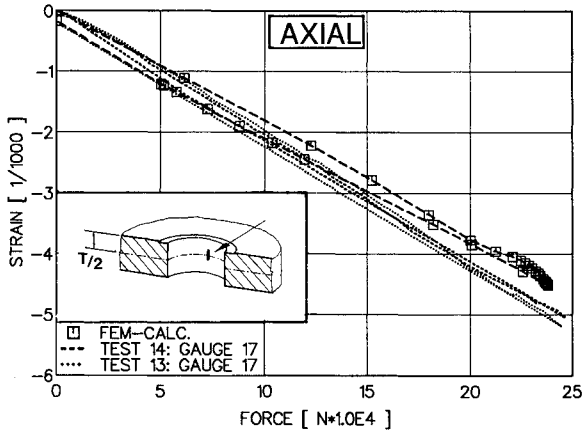

Fig. 8 Measured axial strain ε_{z2} vs coining force for test plates 13, 14 together with corresponding calculated FE-result.

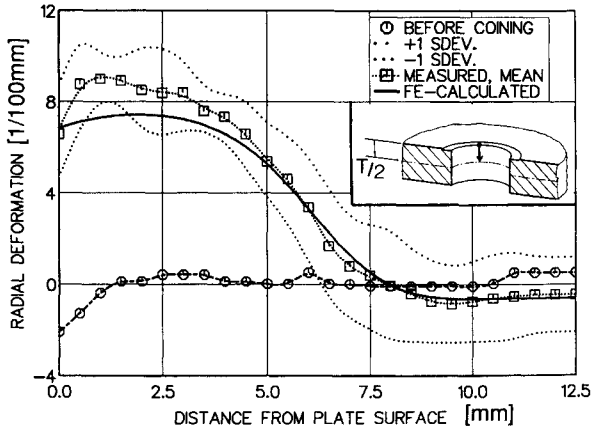

Fig. 9 FE-calculated and measured radial deformations of the hole surface, along a vertical line from the plate surface to half of the plate thickness.

the same locations. Table 1 shows measured mean values and standard deviations.

Computed Stresses Along a Radial Line

Calculated stresses and strains along a radial line from a point on the hole surface, located 5.35 mm below the plate surface, are presented in Figs. 10 and 11. The favorable compressive stresses in the vicinity of the hole surface decline rapidly with increasing radius. About 4 mm inside the hole surface for the 35-mm mandrel and about 8 mm for the 42.5-mm mandrel, the stresses change sign and, instead of being favorable they become adverse. The stress gradient in the zone just below the edge of the mandrel is large, and a tensile stress peak is also observed. Figure 11 shows results for both the case with the mandrel diameter 42.5 mm and 35.0 mm. Both a deeper zone of compressive stresses and larger peak in tensile stresses are found for the larger mandrel.

Factors Governing the Residual Stress Distribution

The influence of controllable coining parameters and geometric properties on the residual tangential stress distribution at the hole surface is here investigated using FEA. The results are shown in Figs. 12–14. Controllable parameters are the coining depth and, to some extent, the friction coefficient. The geometric properties varied are the plate diameter and the mandrel diameter. In Figs. 12–14, the solid lines represent the residual tangential stress-state for the reference FE-computation.

Figure 12 shows how the friction coefficient between the mandrel and the plate affects the residual tangential stresses at the hole surface. The friction coefficient is varied between $My = 0.1$ and $My = 0.4$. At a small distance below the plate surface, from 1 to 5 mm, a noticeable increase in residual stress is obtained when the friction is increased. On the other hand, only small differences are observed closer to the plate surface.

Also the coining depth affects the magnitude and shape of the residual stress state. If the coining depth is decreased more than 30% a significant reduction of the residual tangential stress at the hole surface is observed. For coining depths varying between 0.140 and 0.193 mm an almost constant tangential stress state is obtained on the hole surface (see Fig. 13).

When the diameter of the mandrel is increased the residual tangential stresses become more homogeneous through the thickness (see Fig. 14). The mandrel diameter is varied between 35.0 and 42.5 mm.

No significant effect of a varied plate diameter is observed unless the plate diameter is less than 100 mm.

Table 1 Estimated mean (Mean) values and one standard deviation (SD) for measured strains for tests 5, 6, 13, and 14 for AA6082-T6

	Elastic strains, μstr		Maximum strains, μstr	
Gauge	Mean	SD	Mean	SD
10, 12, 14	−900	210	−2660	950
11, 13, 15	−1140	111	−1520	310

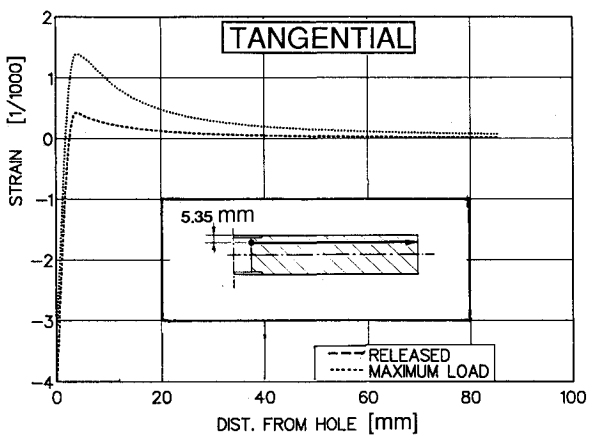

Fig. 10 FE-calculated tangential strains along a radial line oriented from a point at the hole surface towards the outer edge of the plate.

Discussion

A 40% scatter between strain values measured at $\theta = 0$, $\theta = 120$, or $\theta = 240$ deg suggests that neither the aluminum plates nor the coining load are absolutely rotationally symmetric. Thus the estimate mean values for the measured tangential strain at $\theta = 0$, $\theta = 120$, and $\theta = 240$ deg (gauges 10, 12, and 14 and gauges 11, 13, and 15, respectively) are presented in Figs. 5–8. On the other hand, for the axial strain

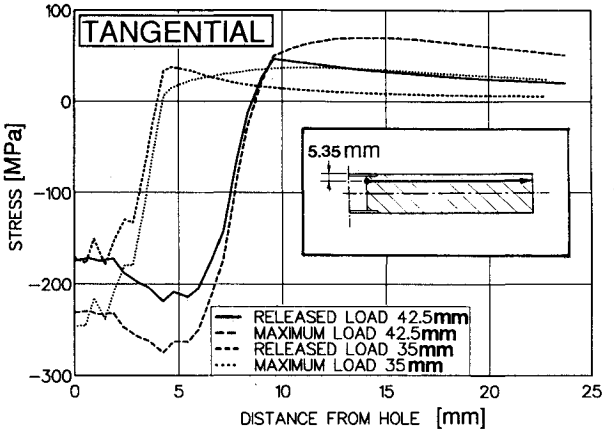

Fig. 11 FE-calculated tangential stresses along a radial line oriented from a point at the hole surface towards the outer edge of the plate for two mandrel diameters, 35 and 42.5 mm.

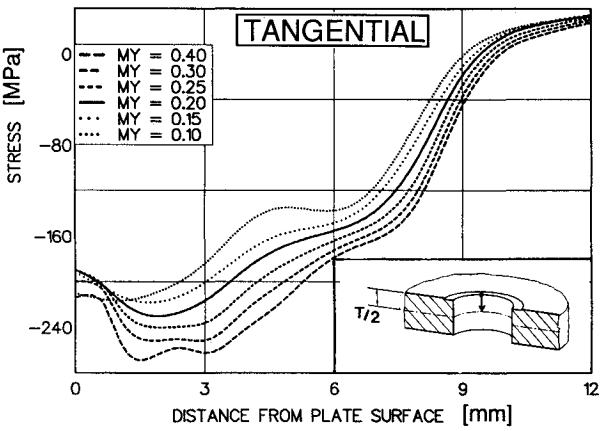

Fig. 12 Influence of the friction coefficient (*MY*) on FE-calculated residual tangential stresses, along a vertical line on the hole surface.

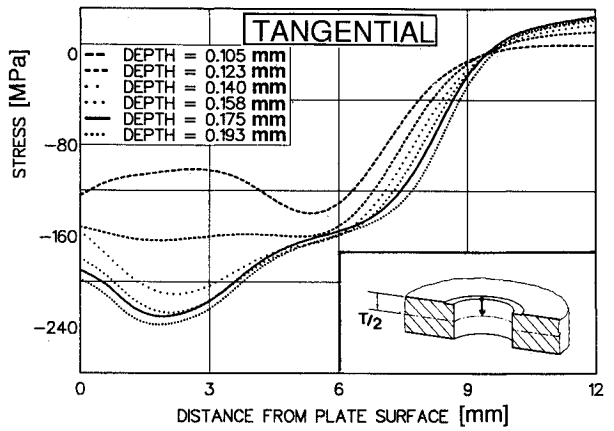

Fig. 13 Influence of the coining depth on FE-calculated residual tangential stresses, along a vertical line on the hole surface.

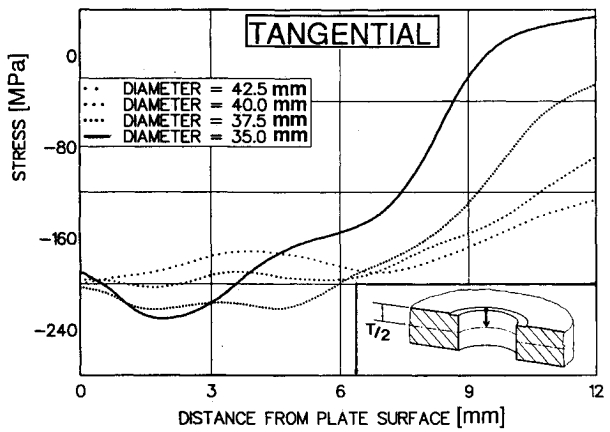

Fig. 14 Influence of the mandrel diameter on FE-calculated residual tangential stresses, along a vertical line on the hole surface.

(gauges 16 and 17) only a single value from each test is presented, and these strain values have to be regarded as more uncertain.

The accuracy of the strain measurements is verified in several elasto-plastic experiments. The strain gauges are capable of accurately measuring strains up to 8% if they are sufficiently bonded to the metal. No failures regarding strain gauges occurred during the tests.

The FE-computed residual strain and stress states seem to be rather insensitive to small changes in: 1) the constitutive material model used for aluminum, 2) the coining depth, and 3) the friction coefficient. On the other hand, to control the residual stress state these parameters are used, but then the changes have to be larger (see Figs. 12–14). This suggests that it may be possible to develop methods which are usable also under conditions less controlled than those in a laboratory experiment.

Due to the large tangential and axial strain gradients present in the axial direction at the hole surface some uncertainties may arise when comparing measured and FE-calculated strains, even if these effects are lowered using mean values estimated over a certain distance.

The nearly straight lines obtained during the unloading phase in Figs. 5–8 suggest that the material is almost elastic during unloading. The agreement between the FE-calculated and the experimental results for the unloading phase is good.

Comparisons with Other Investigations from the Literature

Kasgard et al.[6] have measured residual strains after a similar but not identical coining process. The test plates used by Kasgard et al.[6] had almost the same geometry, but the thickness was 10 mm. They used only two strain gauges on the hole surface but had several strain gauges mounted on the surface of the plate at different radii. They assumed plane stress conditions when the stress state was derived from the measured strains. Hence no axial variations were considered. On the other hand, more information was obtained on the radial variation of the residual strain. When comparing the FE-computed stresses in the present study and the stresses derived from the strain measurements, made by Kasgard et al.[6] one finds, that both the maximum compressive stresses at the hole surface, and the tensile stress peaks are significantly smaller for the FE-computed results than for the experimentally obtained stress. However, the shape of the tangential stress vs radius curve is the same.

Tangential residual stress distributions similar to those presented here can also be obtained using mandrizing methods.[14–16]

Conclusions

Using a nonlinear FE-code, it is possible to predict the tangential and axial strain behavior at the hole surface of an aluminum plate during a coining process. The computed results show that a small displacement and small strain theory is sufficient for these simulations, as long as the coining depth is less than approximately 5% of the plate thickness. Also, the shape of the coined plate can be predicted using a nonlinear FE-code.

The magnitudes of the FE-computed residual tangential stresses depend on: 1) the friction coefficient, 2) the coining depth, and 3) the mandrel diameter. On the other hand, no significant dependency of the plate size can be observed unless the diameter is less than 100 mm. A more favorable stress state (larger compressive tangential stresses) is achieved when the friction coefficient, the coining depth or the mandrel diameter are increased.

Acknowledgments

This research project has been sponsored by Marinteknik Verkstads AB, the National Swedish Board of Technical Development (STU) and the Swedish Ship Builders' Association (SVF). Aluminum Teknik AB has provided me with the aluminum plates needed for the experiments.

The work has been carried out at the Division of Marine Structural Engineering, Chalmers University of Technology.

I thank my supervisor Docent Lennart Josefson at the Division of Solid Mechanics, Chalmers University of Technology and my examiner Professor Anders Ulfvarson at my department for their support during the work. All the experiments were skillfully carried out by Lannart Malm at my department.

References

[1]Gurney, T. R., "Methods of Improving Fatigue Strength," *Fatigue of Welded Structures*, 2nd ed., Cambridge Univ. Press, Cambridge, England, UK, 1979, pp. 301–338.

[2]Jeansson, B., and Larsson, S-E., "Control and Use of Residual Stresses in Aircraft Structural Parts," *Journal of Aircraft*, Vol. 25, No. 1, 1988, pp. 48–54.

[3]Philips, A., "Coining Structural Parts," US Patent 3 110 086, Nov. 1963.

[4]Speakman, E. R., "Fatigue Life Improvement Through Stress Coining Methods," *Achievement of High Fatigue Resistance in Metals and Alloys*, ASTM STP 467, 1970, pp. 209–227.

[5]Speakman, E. R., "Stress Coining," US Patent 3 434 327, March 1969.

[6]Kasgard, P. V., Day, E. E., and Kobayshi, A. S., "Exploratory Study on Optimum Coining for Improvement of Fatigue Life," *Experimental Mechanics*, Vol. 4, Oct. 1964, pp. 297–305.

[7]McNeill, W. A., and Heston, A. W., "Coldworking Fastener Holes—Theoretical Analysis, Methods of Coldworking, Experimental Results," *Proceedings of the Conference on Residual Stress in Design, Process and Materials Selections*, ASM International, Cincinnati, OH, April 27–29, 1987, pp. 193–204.

[8]Armen, H., Levy, A., and Eidinoff, H. L., "Elastic-Plastic Behavior of Coldworked Holes," *Journal of Aircraft*, Vol. 21, No. 3, 1984, pp. 193–201.

[9]Nadai, A., "Theory of the Expanding of Boiler and Condenser Tube Joints Through Rolling," *Transactions of the American Society of Mechanical Engineers*, Vol. 65, Nov. 1943, pp. 865–880.

[10]Ogeman, R., "Coining of Holes in Aluminum Plates, Finite Element Simulations and Experiments," Div. of Marine Structural Engineering, Chalmers Univ. of Technology, CHA/NAV/R-90/0012, Göteborg, Sweden, Nov. 1990.

[11]"SOLVIA-PRE, User's Manual," SOLVIA Engineering AB, Rept. SE-1, Västerås, Sweden, 1990.

[12]Bathe, K.-J. and Chaudhary, A., "A Solution Method for Planar and Axisymmetric Contact Problems," *International Journal for Numerical Methods in Engineering*, Vol. 21, No. 1, 1985, pp. 65–88.

[13]Mazzolani, F. M., "The Structural Material," *Aluminum Alloy Structures*, 1st ed., Pitman, Boston, 1985, pp. 52–126.

[14]Yen, S. W., "Theory of Stress Coining Technique," *Engineering Fracture Mechanics*, Vol. 14, No. 3, 1981, pp. 477–491.

[15]Su, X., Gu, M., and Yan, M., "A Simplified Residual Stress Model for Predicting Fatigue Crack Growth Behavior at Coldworked Fastener Holes," *Fatigue & Fracture of Engineering Materials & Structures*, Vol. 9, No. 1, 1986, pp. 57–64.

[16]Hsu, Y. C., and Forman, R. G., "Elastic-Plastic Analysis of an Infinite Sheet Having a Circular Hole Under Pressure," *ASME Journal of Applied Mechanics*, Vol. 42, No. 2, 1975, pp. 347–352.